Letter | Editors' Suggestion

One-dimensional projection of two-dimensional systems using spiral boundary conditions

Masahiro Kadosawa,[1] Masaaki Nakamura,[2] Yukinori Ohta,[1] and Satoshi Nishimoto[3,4]
[1]*Department of Physics, Chiba University, Chiba 263-8522, Japan*
[2]*Department of Physics, Ehime University, Ehime 790-8577, Japan*
[3]*Department of Physics, Technical University Dresden, 01069 Dresden, Germany*
[4]*Institute for Theoretical Solid State Physics, IFW Dresden, 01069 Dresden, Germany*

(Received 31 May 2022; accepted 25 January 2023; published 9 February 2023)

We introduce spiral boundary conditions (SBCs) as a useful tool for handling the shape of finite-size periodic clusters. Using SBCs, a lattice model for more than two dimensions can be exactly projected onto a one-dimensional (1D) periodic chain with translational invariance. Hence, the existing 1D techniques such as density-matrix renormalization group (DMRG), bosonization, Jordan-Wigner transformation, etc., can be effectively applied to the projected 1D model. First, we describe the 1D projection scheme for the two-dimensional (2D) square- and honeycomb-lattice tight-binding models in real and momentum space. Next, we discuss how the density of states and the ground-state energy approach their thermodynamic limits. Finally, to demonstrate the utility of SBCs in DMRG simulations, we estimate the magnitude of staggered magnetization of the 2D XXZ Heisenberg model as a function of XXZ anisotropy.

DOI: 10.1103/PhysRevB.107.L081104

Introduction. In condensed matter physics, theoretical research is usually carried out based on the statistical mechanical formulation of either lattice or continuum models which describe the microscopic structure of solids. In general, a lattice model is a cluster of lattice points corresponding to the positions of aligned atoms in a crystal [1]. The Hamiltonian is typically expressed as a countable set of lattice points or bonds, because finite degrees of freedom such as spin, charge, hole, etc., are assigned in each lattice point. Therefore, unlike in the continuum limit with huge degrees of freedom, a lattice model is rather suitable for computer simulations. Typical examples of a lattice model are the Hubbard model [2], the Heisenberg model [3], the Kondo-lattice model [4], and the Kitaev model [5]. A microscopic starting point to understand the electronic and/or magnetic properties of solids is provided by solving those kinds of lattice models analytically or numerically.

When studying such a model in numerical simulations, we usually put it on a lattice of finite size. Then, an extrapolation of the result to an infinite system is considered if necessary. However, since the total degrees of freedom of the system increases exponentially with lattice size, the geometry of the cluster can be strongly restricted especially for systems in more than two dimensions. In such cases, the management of boundary conditions is crucial to ensure "correct" simulations. Either periodic boundary conditions (PBCs), open boundary conditions (OBCs), or a combination of them, such as, e.g., a cylinder, are typically used. Nevertheless, a naive choice of boundary conditions could easily give rise to a situation where the lowest-energy state with a small cluster is not relevant to the ground state (GS) in the thermodynamic limit, instead of systematic errors due to the finite-size effects. This issue could be addressed for example by the sorting of states with, e.g., quantum numbers, momentum, and parity, as explicitly done in level spectroscopy [6], or by controlling the open edges for a particular state [7]. However, these approaches are not always successful.

A simple alternative way to resolve or reduce the above issue is by the use of spiral boundary conditions (SBCs). As explained below, SBCs enable us to represent two-dimensional (2D) lattice sites by a one-dimensional (1D) array. This method was originally used to optimize the computational cost in Monte Carlo simulations [8] but it also allows us to efficiently apply existing 1D techniques such as the density-matrix renormalization group (DMRG) [9], bosonization [10], and Jordan-Wigner transformation [11], etc. SBCs have been also introduced for extending the Lieb-Schultz-Mattis theorem to higher dimensions [12] and for discussing the GS degeneracy in the thermodynamic limit [13]. In this Letter, we thus propose SBCs as a useful tool for handling the shape of finite-size periodic clusters. As practical examples, we describe the 1D projections of the 2D square- and honeycomb-lattice tight-binding (TB) models in real and momentum space. Then, we present how the density of states (DOS) and the GS energy approach their thermodynamic limits. Furthermore, in order to demonstrate the utility of SBCs, we calculate the GS energy of the 2D half-filled Hubbard model and the magnitude of staggered magnetization of the 2D XXZ Heisenberg model using the DMRG method. Their estimations had been longstanding problems and were only recently settled [14,15]. In our DMRG calculations, we keep up to 12 000 density-matrix eigenstates and the typical discarded weight is smaller than $\sim 10^{-5}$. More detailed data are given in the Supplemental Material [16].

Projection of 2D cluster onto 1D chain using SBCs. SBCs are a variation of the idea of PBCs. They provide a way to

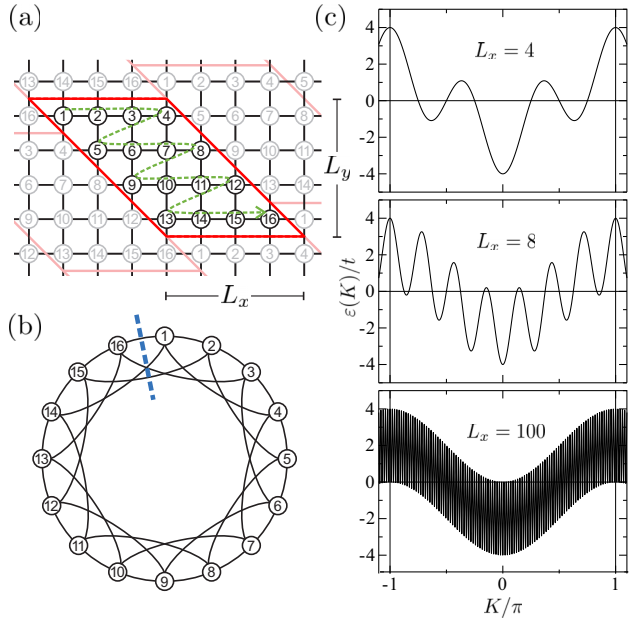

FIG. 1. (a) 2D square-lattice cluster with 4×4 sites, where the region framed by the red line is the original cluster. (b) 1D representation of the cluster (a) by numbering sites along the green line. This is a periodic chain, and an open chain is created by cutting L_x bonds between two sites (dotted line). (c) L_x dependence of the energy dispersion $\varepsilon(K)$, where the limit $L_y \to \infty$ is taken.

map lattice models for more than two dimensions onto 1D periodic chains with translation symmetry. As an illustration, let us consider the TB model on a square lattice with $L_x \times L_y$ sites. When a PBC is applied to its finite-size system, we usually use a rectangular cluster and sites on one edge of the cluster are assumed to be neighbors of the corresponding sites on the opposite edge. However, this choice may be arbitrarily deformed as long as the boundaries have the correct topology of state. Thus, we now make a particular choice of boundaries shown in Fig. 1(a), where all sites are traced along the dashed line in a spiral manner. In this way, the original 2D cluster can be exactly reproduced as a 1D chain with nearest- and $(L_x - 1)$th-neighbor hopping integrals [Fig. 1(b)], where the translational symmetry is preserved. The Hamiltonian is written as $\mathcal{H}_{\mathrm{sq},0} = -t \sum_\sigma \sum_{i=1}^{L_x L_y} (c_{i,\sigma}^\dagger c_{i+1,\sigma} + c_{i,\sigma}^\dagger c_{i+(L_x-1),\sigma} + \mathrm{H.c.})$, where $c_{i,\sigma}$ is an annihilation operator of an electron with spin σ at site i, and t is the nearest-neighbor hopping integral in the original 2D model. Its Fourier transform leads to $\mathcal{H}_{\mathrm{sq},K} = -2t \sum_{K,\sigma} [\cos K + \cos(L_x - 1)K] c_{K,\sigma}^\dagger c_{K,\sigma}$, where K is the momentum defined along the projected 1D periodic chain and $c_{K,\sigma} = (1/\sqrt{L_x L_y}) \sum_i \exp(iKr_i) c_{i,\sigma}$. Since the sites are ordered along a "snakelike" path shown in Fig. 1(a), the original 2D momenta $(k_x, k_y) = (\frac{2\pi}{L_x} n_x, \frac{2\pi}{L_y} n_y)$ $(n_x = 0, 1, \ldots, L_x - 1;$ $n_y = 0, 1, \ldots, L_y - 1)$ are transferred to the 1D momentum $K = \frac{2\pi}{L_x L_y} n$ with $n = n_x + L_x n_y = 0, 1, \ldots, L_x L_y - 1$.

The L_x dependence of the energy dispersion $\varepsilon(K) = -2t[\cos K + \cos(L_x - 1)K]$ is shown in Fig. 1(c), where the limit $L_y \to \infty$ is taken to obtain a continuous dispersion with K. Reflecting the snakelike order of sites in the original 2D cluster, the dispersion is oscillating as a function of K. In the large L_x limit it turns out to be a beltlike dispersion relation which is interpreted as the projected band structure of the square-lattice TB model onto a Cartesian axis, i.e., x or y. The original 2D Fermi surface is represented as a "Fermi line." For example, when the Fermi level is set at $0 < \varepsilon_F < 4$, two separate unoccupied regions correspond to the hole pockets.

Let us see the case of half filling. The dispersion is particle-hole symmetric and there are $2L_x - 2$ Fermi points. The GS energy E_0 can be calculated by carrying out the single-particle energy summation over the $L_x - 1$ regions with $\varepsilon(K) < 0$,

$$\frac{E_0}{L_x L_y} = -\frac{4}{\pi} \int_{\varepsilon(K)<0} (\cos K + \cos[(L_x - 1)K]) dK \quad (1)$$

$$= -\frac{4}{\pi} \sum_{j=1}^{L_x/2} \left[\sin K + \frac{\sin[(L_x - 1)K]}{L_x - 1} \right]_a^b$$

$$\xrightarrow[L_x, L_y \to \infty]{} -\frac{16}{\pi^2}, \quad (2)$$

where $a = \min(0, \frac{2j-3}{L_x - 2}\pi)$ and $b = \frac{2j-1}{L_x}\pi$. This energy coincides with that of the infinite-size system. Therefore, we can confirm that the finite-size systems under SBCs are adiabatically connected to the thermodynamic limit. More details are given in the Supplemental Material [16].

Note that the way of 1D projection using SBCs is not unique. This means that the modulation of the wave function can be controlled more flexibly than PBCs [17]. In other words, a periodic system consistent with an arbitrary commensurate ordering vector can be created by tuning the shape of the finite-size cluster and its alignment. Similar boundary conditions have been used in some numerical calculations to manage a limited periodicity of small clusters [18,19]. Other examples of SBC usage are given in the Supplemental Material [16].

Honeycomb-lattice TB model under SBCs. Another interesting example is the honeycomb-lattice TB model. The choice of spiral boundaries and the corresponding projected 1D chain are shown in Figs. 2(a) and 2(b), respectively. The Hamiltonian of the projected 1D chain is written as $\mathcal{H}_{\mathrm{hon},0} = -t \sum_{i=1}^{L_x L_y} \sum_\sigma (c_{2i-1,\sigma}^\dagger c_{2i,\sigma} + c_{2i,\sigma}^\dagger c_{2i+1,\sigma} + c_{2i,\sigma}^\dagger c_{2i+(2L_x-1),\sigma} + \mathrm{H.c.})$. For the limit of $L_y \to \infty$ the energy dispersion is written as $\varepsilon(K) = \pm t \sqrt{1 + 4\cos^2 \frac{K}{2} + 4 \cos \frac{K}{2} \cos \frac{(2L_x-1)K}{2}}$. The L_x dependence of $\varepsilon(K)$ is shown in Fig. 2(c). The upper and lower bands are degenerate at $K = \pm\frac{2}{3}\pi$ only when $2L_x - 1 = 3M$, where M is an integer. In the limit of $L_x, L_y \to \infty$, the band structure is equivalent to the projected one of 2D graphene onto a zigzag axis. Accordingly, the Dirac points of the original 2D graphene are reproduced at $K = \pm\frac{2}{3}\pi$.

Approach to the thermodynamic limit. It is informative to see how the DOS and the GS energy approach their thermodynamic limits. For simplicity, hereafter we consider the case of $L_x = L_y = L$. The evolution of the DOS with L for the square- and honeycomb-lattice TB models is shown in Figs. 3(a) and 3(b), respectively. With increasing L, they are smoothly connected to the thermodynamic limit ones. Also, the overall shape including the van Hove singularity can be approximately reproduced even with a relatively small cluster. It is because the degeneracy of the energy levels in a finite-

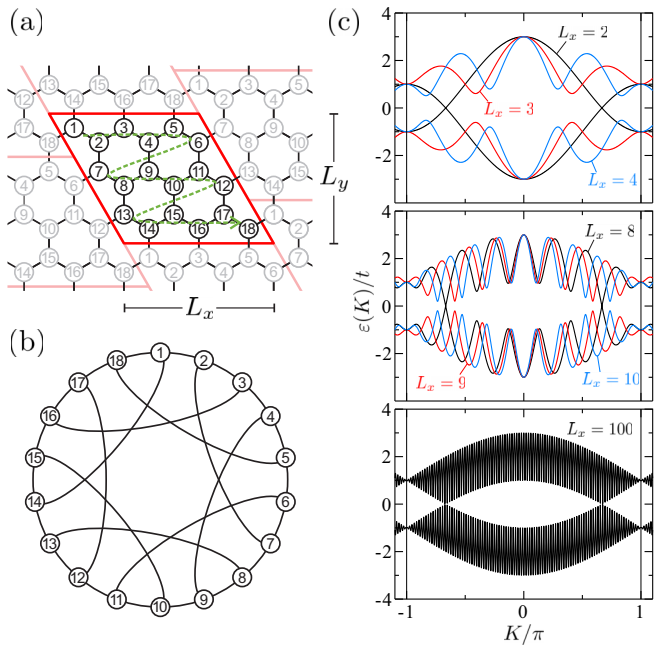

FIG. 2. (a) 2D honeycomb-lattice cluster with 3×3 unit cells, where a region framed by the red line is the original cluster. (b) 1D representation of the cluster (a) by numbering sites along the green line. (c) L_x dependence of the energy dispersion $\varepsilon(K)$, where the limit $L_y \to \infty$ is taken. The upper and lower bands are degenerate at $K = \pm\frac{2}{3}\pi$ when $2L_x - 1 = 3M$ (M: integer).

size PBC cluster is lifted due to the partial breaking of its rotation symmetry by SBCs. For a square-lattice cluster with $L \times L$ sites, the number of independent momenta is $\frac{L^2}{2} + 1$ under SBCs and $\frac{L^2}{8} + \frac{3L}{4} + 1$ under PBCs. More details are discussed in the Supplemental Material [16].

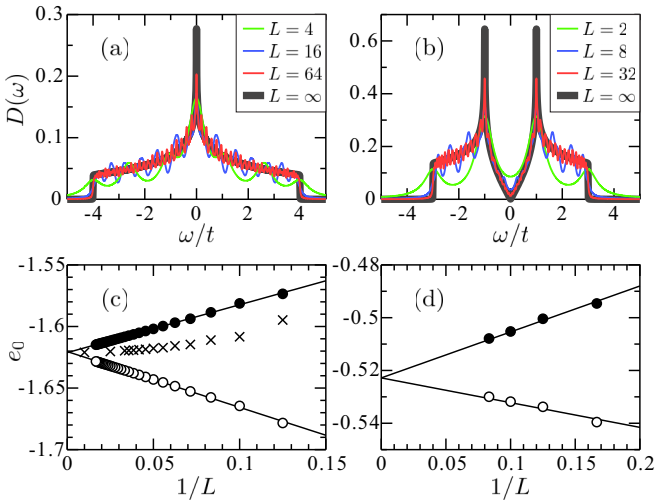

FIG. 3. L dependence of the density of states for (a) square- and (b) honeycomb-lattice TB models, where a broadening of the δ peak $1.6/L$ and $0.8/L$ is introduced, respectively. Finite-size scaling analysis of the ground-state energy for the half-filled square-lattice Hubbard model at (c) $U = 0$ and (d) $U/t = 8$. Solid and open circles denote the energy per two bonds and per site calculated with open chains, respectively. Crosses denote the energy per site calculated with periodic chains.

In Fig. 3(c) a finite-size scaling analysis of the GS energy for the half-filled square-lattice TB model with the projected 1D periodic chains is shown. The data points are analytically obtained. As expected, the energy per site (e_0) quadratically approaches $-\frac{16}{\pi^2}$ as a function of $\frac{1}{L}$. It is also interesting to see the scaling behavior when open chains are used. An open chain is created by cutting L bonds between two neighboring sites of the periodic chain [see Fig. 1(b)]. Note though that the number of missing bonds is reduced from $2L$ in the original 2D PBC cluster to L. Nevertheless, since the ratio of the number of bonds per site deviates from 2 due to the missing bonds for finite-size open chains, it is convenient to estimate the GS energy in two different ways: One is the energy per site and the other is that per two bonds. As shown in Fig. 3(c), both of them are extrapolated almost linearly to the thermodynamic limit. One of them is extrapolated from the higher-energy side with decreasing $\frac{1}{L}$ and the other from the lower-energy side, so that this makes the scaling analysis more reliable. Eventually, the scaling behavior with open chains seems to be even more simple than that with periodic chains.

Application of SBCs in DMRG calculations. In DMRG simulations for a 2D system, it is not easy to obtain physical quantities in the thermodynamic limit because not only are their implementations challenging even with finite-size clusters, but also the finite-size scaling analysis must be performed along two orientations, e.g., the x and y directions. This issue can be somewhat alleviated by applying the above 1D projection scheme. In order to demonstrate this, we here present two examples of DMRG simulations for a 2D system.

The first example is the GS energy of the 2D half-filled Hubbard model on a square lattice, whose Hamiltonian is $\mathcal{H} = \mathcal{H}_{\mathrm{sq},0} + U\sum_i n_{i,\uparrow}n_{i,\downarrow}$, where $n_{i,\sigma} = c^\dagger_{i,\sigma}c_{i,\sigma}$. In Fig. 3(d) the finite-size scaling of GS energy for $U = 8$ is performed. As is the case in the TB model, open chains are used, so that the extrapolation to the thermodynamic limit seems to be straightforward. It leads to $e_0 = -0.5228$ by linear fitting. This energy is only slightly higher than $e_0 = -0.5241$ estimated by DMRG calculations with infinite-length cylinders [14]. Perhaps the extrapolation in the circumferential direction may contain some uncertainty due to the unsettled scaling function with several data points.

The second example is the spontaneous staggered magnetization of the 2D XXZ Heisenberg model on a square lattice, whose Hamiltonian is $\mathcal{H} = \sum_{\langle i,j\rangle}(S^x_iS^x_j + S^y_iS^y_j + \Delta S^z_iS^z_j)$, where S^γ_i are the spin-$\frac{1}{2}$ operators associated with site i, Δ is the anisotropy parameter, and the sum $\langle i, j\rangle$ runs over all nearest-neighbor pairs. We here use periodic chains. As sketched in Fig. 4(a), the z components of spins at sites i and $i+1$ are fixed to $\frac{1}{2}$ and $-\frac{1}{2}$, respectively, and the spin moments at the farthest two sites from the fixed spins are measured: $m^{\mathrm{st}}_z = -\langle S^z_{i+1+\frac{N}{2}}\rangle = \langle S^z_{i+\frac{N}{2}}\rangle$. Several examples of the finite-size scaling analysis are shown in Fig. 4(b), where the spin moments are calculated using periodic chains with lengths up to $N = L^2 = 100$ sites. For the isotropic case ($\Delta = 1$), we obtain $m^{\mathrm{st}}_z = 0.3071 \pm 0.0005$ in the thermodynamic limit. This value is reasonably close to the previous DMRG ($m^{\mathrm{st}}_z = 0.3067$) [20] and

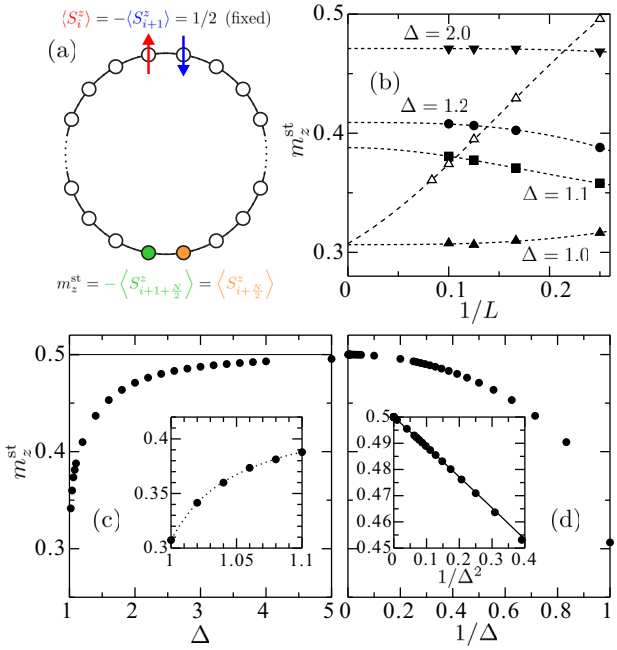

FIG. 4. (a) Schematic picture of the 1D periodic chain used for the DMRG calculations of staggered magnetization m_z^{st}. (b) Finite-size scaling analysis of m_z^{st}. Solid symbols denote the data points estimated with spin rotation symmetry breaking, and open triangles denote those estimated from the static structure factor (see text). (c), (d) Extrapolated values of m_z^{st} in the thermodynamic limit. Insets: Enlarged views near $\Delta = 1$ and $1/\Delta = 0$, respectively. The solid line in the inset of (d) shows a fitting by a polynomial function with $1/\Delta$.

quantum Monte Carlo ($m_z^{\mathrm{st}} = 0.307\,43$) [15] estimations. The magnetization increases with increasing Δ. The extrapolated values of m_z^{st} are plotted as a function of Δ in Fig. 4(c). The overall behavior is basically consistent with the previous studies [21–24]. However, a singularity near $\Delta = 1$, $m_z^{\mathrm{st}} = \sum_{n=0}^{\infty} \mu_n (1-\Delta^{-2})^{n/2}$, predicted by the spin-wave theory [21,25,26] is not confirmed in our results. This is consistent with results from the coupled cluster method [24]. A more detailed analysis is given in Ref. [27]. On the other hand, as shown in Fig. 4(d), our data in the large-Δ region ($0 \leqslant 1/\Delta \leqslant 0.05$) can be fitted by $2m_z^{\mathrm{st}} = 1 + m_2/\Delta^2 + m_4/\Delta^4 + m_6/\Delta^6$ with $m_2 = -0.222\,222\,225$, $m_4 = -0.035\,554\,273\,6$, and $m_6 = -0.018\,966\,381\,0$. This agrees well with the series expansions $2m_z^{\mathrm{st}} = 1 - (2/9)/\Delta^2 - (8/225)/\Delta^4 - 0.018\,942\,58/\Delta^6 + O(1/\Delta^8)$ ($2/9 = 0.222\,222\,22\ldots$, $8/225 = 0.035\,555\,5\ldots$) [21].

Finally, we present another option to calculate the staggered magnetization. In the above estimations, the spin rotation symmetry is broken by design. Although it makes the DMRG calculations more stable, an equally precise estimation of m_z^{st} is also possible without such explicit symmetry breaking. Using open chains, we can accurately estimate the staggered magnetization from the static structure factor $(m_z^{\mathrm{st}})^2 = \lim_{L\to\infty}(1/L^2)\sum_{ij}(-1)^{i-j}\langle \boldsymbol{S}_i \cdot \boldsymbol{S}_j\rangle$, where the sum is taken over the open chain. The finite-size scaling analysis using the chains with lengths up to 12×12 is given in Fig. 4(b). We obtain $m_z^{\mathrm{st}} = 0.307\,62 \pm 0.0032$ in the thermodynamic limit.

Summary. Applying SBCs, lattice models for more than two dimensions can be exactly projected onto 1D periodic chains with translational invariance. In the projected 1D chain, each lattice site is indexed by a single coordinate instead of two coordinates in the original 2D PBC cluster, so that we only have to perform a finite-size scaling analysis along the chain direction to obtain a physical quantity in the thermodynamic limit. As practical examples, we first explained how the 2D square- and honeycomb-lattice TB models are expressed as 1D periodic systems in both real and momentum space. Then, the evolution of the DOS with increasing cluster size as well as a finite-size scaling analysis of the GS energy to the thermodynamic limit was shown. Finally, in order to demonstrate the utility of this 1D projection scheme in DMRG simulations, we calculated the magnitude of staggered magnetization in the 2D XXZ Heisenberg model on a square lattice.

The 1D projection scheme using SBCs can be extended to further research. Since the projected 1D chain has translational symmetry, all of the so-called (local) A tensors are set to be equivalent in a matrix product state. As a result, quantum entanglement is uniformly distributed over the projected 1D chain. It is also important that the distance of the longest bonds is minimized. These conditions enable us to optimally perform DMRG calculations, and also allow us to use the existing techniques such as infinite DMRG and transfer-matrix renormalization group. Though only two kinds of 2D lattices are considered in this Letter, a similar 1D projection is possible for any periodic lattices in more than two dimensions [8]. Moreover, in most cases SBCs are expected to practically give an easier finite-size scaling analysis than the cylinder and PBCs. To clarify the advantages of SBCs in DMRG simulations, the comparison of performance with other boundary conditions is discussed in the Supplemental Material [16].

Acknowledgments. We thank Ulrike Nitzsche for technical support. This work was supported by Grants-in-Aid for Scientific Research from JSPS (Projects No. JP20H01849, No. JP20K03769, and No. JP21J20604). M.K. acknowledges support from the JSPS Research Fellowship for Young Scientists. M.N. acknowledges support from the Visiting Researcher's Program of the Institute for Solid State Physics, The University of Tokyo, and the research fellow position of the Institute of Industrial Science, The University of Tokyo. S.N. acknowledges support from SFB 1143 project A05 (Project-Id 247310070) of the Deutsche Forschungsgemeinschaft.

[1] N. W. Ashcroft and N. D. Mermin, *Solid State Physics* (Saunders College Publishing, Philadelphia, 1976).

[2] J. Hubbard, Electron correlations in narrow energy bands, Proc. R. Soc. London, Ser. A **276**, 238 (1963).

[3] W. J. Heisenberg, Zur theorie des ferromagnetismus, Z. Phys. **49**, 619 (1928).

[4] J. Kondo, Resistance minimum in dilute magnetic alloys, Prog. Theor. Phys. **32**, 37 (1964).

[5] A. Kitaev, Anyons in an exactly solved model and beyond, Ann. Phys. **321**, 2 (2006).

[6] K. Okamoto and K. Nomura, Fluid-dimer critical point in $S = 1/2$ antiferromagnetic Heisenberg chain with next nearest neighbor interactions, Phys. Lett. A **169**, 433 (1992).

[7] S. Nishimoto and M. Nakamura, Non-symmetry-breaking ground state of the $S = 1$ Heisenberg model on the kagome lattice, Phys. Rev. B **92**, 140412(R) (2015).

[8] M. E. Newman and G. T. Barkema, *Monte Carlo Methods in Statistical Physics* (Clarendon Press, Oxford, UK, 1999).

[9] S. R. White, Density matrix formulation for quantum renormalization groups, Phys. Rev. Lett. **69**, 2863 (1992).

[10] A. O. Gogolin, A. A. Nersesyan, and A. M. Tsvelik, *Bosonization and Strongly Correlated Systems* (Cambridge University Press, Cambridge, UK, 2004).

[11] H.-D. Chen and Z. Nussinov, Exact results of the Kitaev model on a hexagonal lattice: Spin states, string and brane correlators, and anyonic excitations, J. Phys. A: Math. Theor. **41**, 075001 (2008).

[12] Y. Yao and M. Oshikawa, Generalized Boundary Condition Applied to Lieb-Schultz-Mattis-Type Ingappabilities and Many-Body Chern Numbers, Phys. Rev. X **10**, 031008 (2020).

[13] M. G. Yamada and S. Fujimoto, Thermodynamic signature of SU(4) spin-orbital liquid and symmetry fractionalization from Lieb-Schultz-Mattis theorem, Phys. Rev. B **105**, L201115 (2022).

[14] J. P. F. LeBlanc, A. E. Antipov, F. Becca, I. W. Bulik, G. K.-L. Chan, C.-M. Chung, Y. Deng, M. Ferrero, T. M. Henderson, C. A. Jiménez-Hoyos, E. Kozik, X.-W. Liu, A. J. Millis, N. V. Prokof'ev, M. Qin, G. E. Scuseria, H. Shi, B. V. Svistunov, L. F. Tocchio, I. S. Tupitsyn *et al.* (Simons Collaboration on the Many-Electron Problem), Solutions of the Two-Dimensional Hubbard Model: Benchmarks and Results from a Wide Range of Numerical Algorithms, Phys. Rev. X **5**, 041041 (2015).

[15] A. W. Sandvik and H. G. Evertz, Loop updates for variational and projector quantum Monte Carlo simulations in the valence-bond basis, Phys. Rev. B **82**, 024407 (2010).

[16] See Supplemental Material at http://link.aps.org/supplemental/10.1103/PhysRevB.107.L081104 for a detailed analysis of the ground-state energy of the 2D square-lattice tight bonding model. Also, the difference of the momentum distribution between periodic and spiral boundary conditions is discussed. In addition, the detailed data of our DMRG calculations with spiral boundary conditions are compared to those with various boundary conditions. Finally, the possible advantage of spiral boundary conditions in DMRG simulation is discussed.

[17] M. Nakamura, S. Masuda, and S. Nishimoto, Characterization of topological insulators based on the electronic polarization with spiral boundary conditions, Phys. Rev. B **104**, L121114 (2021).

[18] Y. Nishiyama, Deconfinement criticality in the spatially anisotropic triangular antiferromagnet with ring exchange, Phys. Rev. B **79**, 054425 (2009).

[19] A. Miyata, T. Hikihara, S. Furukawa, R. K. Kremer, S. Zherlitsyn, and J. Wosnitza, Magnetoelastic study on the frustrated quasi-one-dimensional spin-$\frac{1}{2}$ magnet $LiCuVO_4$, Phys. Rev. B **103**, 014411 (2021).

[20] S. R. White and A. L. Chernyshev, Neél Order in Square and Triangular Lattice Heisenberg Models, Phys. Rev. Lett. **99**, 127004 (2007).

[21] Z. Weihong, J. Oitmaa, and C. J. Hamer, Square-lattice Heisenberg antiferromagnet at $T = 0$, Phys. Rev. B **43**, 8321 (1991).

[22] C. J. Hamer, Z. Weihong, and P. Arndt, Third-order spin-wave theory for the Heisenberg antiferromagnet, Phys. Rev. B **46**, 6276 (1992).

[23] H.-Q. Lin, J. S. Flynn, and D. D. Betts, Exact diagonalization and quantum Monte Carlo study of the spin-$\frac{1}{2}$XXZ model on the square lattice, Phys. Rev. B **64**, 214411 (2001).

[24] R. Bishop, P. Li, R. Zinke, R. Darradi, J. Richter, D. Farnell, and J. Schulenburg, The spin-half XXZ antiferromagnet on the square lattice revisited: A high-order coupled cluster treatment, J. Magn. Magn. Mater. **428**, 178 (2017).

[25] Z. Weihong, J. Oitmaa, and C. J. Hamer, Second-order spin-wave results for the quantum XXZ and XY models with anisotropy, Phys. Rev. B **44**, 11869 (1991).

[26] D. A. Huse, Ground-state staggered magnetization of two-dimensional quantum Heisenberg antiferromagnets, Phys. Rev. B **37**, 2380 (1988).

[27] M. Kadosawa, M. Nakamura, Y. Ohta, and S. Nishimoto, Study of staggered magnetization in the spin-S square-lattice Heisenberg model using spiral boundary conditions, J. Phys. Soc. Jpn. **92**, 023701 (2023).